CHEMISTRY
A European Journal

A Journal of
ChemPubSoc Europe

Accepted Article

Title: Upconverting Carbon Nanodots from EDTA as Near-Infrared Activated Phototheranostic Agents

Authors: M. Carmen Ortega-Liebana, M.Mar Encabo-Berzosa, Alvaro Casanova, M. Desiree Pereboom, Octavio Alda, Jose Luis Hueso, and Jesus Santamaria

To be cited as: *Chem. Eur. J.* 10.1002/chem.201806307

Link to VoR: http://dx.doi.org/10.1002/chem.201806307

Supported by
ACES

WILEY-VCH

10.1002/chem.201806307

WILEY-VCH

Upconverting Carbon Nanodots from EDTA as Near-Infrared Activated Phototheranostic Agents

M. Carmen Ortega-Liebana[a, b], M. Mar Encabo-Berzosa[a ,b], Alvaro Casanova[c], M. Desiree Pereboom[c], J. Octavio Alda[c], Jose L. Hueso*[a,b], Jesus Santamaria*[a,b]

Abstract: This work describes the synthesis of nitrogen-doped carbon nanodots (CNDs) synthesized from ethylene diamine tetra acetic acid (EDTA) as a precursor and their application as luminescent agents with a dual-mode theranostic role as near-infrared (NIR) triggered imaging and photodynamic therapy agents. Interestingly, these fluorescent CNDs are more rapidly and selectively internalized in tumor cells and exhibit very limited cytotoxicity until remotely activated with a NIR illumination source. These CNDs are excellent candidates for photo-theranostic purposes, i.e.: simultaneous imaging and therapy can be carried out on cancer cells using their luminescent properties and the *in situ* generation of reactive oxidative species (ROS) upon excitation in the NIR range. In the presence of CNDs NIR remote activation induces the in vitro killing of U251 MG cells. Through the use of flow imaging cytometry we have been able to successfully map and quantify the different type of cell deaths induced by the presence of intracellular superoxide anions ($^{\bullet}O_2^-$) and hydrogen peroxide (H_2O_2) ROS species generated *in situ* upon NIR irradiation.

INTRODUCTION

Phototheranostics has emerged as a novel strategy combining diagnosis and treatment of cancer using photosensitizing agents that are able to in situ generate reactive oxidative species (ROS) while providing a fluorescent response upon the sole irradiation of an orthogonal stimulus with high spatiotemporal resolution such as light. The most widespread photodynamic therapy (PDT) agents are porphyrins, phthalocyanines or bacteriochlorin derivatives co-encapsulated with other fluorescent agents[1, 2]. These systems are typically hydrophobic and suffer from shallow tissue penetration, limited PDT efficiency and restricted excitation wavelengths typically located in the blue and red ranges where the penetration depth of light is hindered. To overcome these drawbacks, recent studies have reported on the use of alternative nanomaterials such as gold nanomaterials[1-3], semiconducting quantum dots[4], semiconducting polymers[5], sulfide-based nanocrystals[6], silica nanoparticles[7] and rare-earth based upconverting inorganic particles[8-10]. These materials have been used as co-photosensitizers (i.e. PDT amplifiers accompanying other sensitizing organic agents) or as light-harvesters in the red and near-infrared (NIR) ranges to favor the deeper penetration of light in the NIR transparent tissue window[1]. Nevertheless, all these alternative sensitizers still face limitations in terms of intrinsic cytotoxicity, colloidal stability, the use of scarce and expensive precursors or the need of highly complex and time-consuming synthesis and purification protocols.

In this regard, carbon-based nanomaterials such as carbon nanotubes and fullerenes have recently shown high potential as alternative photo-sensitizers for combined Photothermal and Photodynamic therapy treatments that can partially overcome the shortcomings of current NIR phototheranostic agents[1]. Likewise, smaller carbogenic members of the carbon family such as nanodiamonds, polymer nanodots, graphene-like dots or carbon nanodots (CNDs) have emerged as novel fluorescent nanosensitizers[11-13] that combine a series of appealing properties such as: (i) high colloidal stability in water and physiological media; (ii) high photo-stability and resistance to photobleaching; (iii) reduced toxicity in comparison with nanosystems containing heavy and potentially toxic elements; (iv) tunable optical response spanning from UV to NIR ranges including large two-photon excitation cross-sections; (v) abundance of inexpensive raw precursors for their synthesis; (vi) facile and straightforward synthesis protocols. A number of recent studies have successfully reported the use of these carbogenic nanostructures as dual-mode imaging and PDT agents, mostly referred to graphene-like dots or functionalized nanodiamonds [1, 4, 14-33].

Herein we report on the use of CNDs synthesized by the hydrothermal carbonization (HTC) of ethylene diamine tetraacetic acid (EDTA) at 260 ºC (see Experimental Section for further details). This molecular precursor has been selected to induce the direct generation of Nitrogen-doped carbon nanodots (N-CNDs) in a single step without the need of secondary amine co-reactants[34-37]. Previous works have claimed that partial substitution of N within the pseudo-graphitic structure of CNDs provides them with expanded photoluminescence response[34-42]. In this work, we demonstrate that the N-CNDs retrieved from EDTA exhibit excellent optical photoluminescence (PL) properties in the whole UV-Vis-NIR range. Furthermore, we show their potential as multimodal theranostic agents in the NIR

[a] Dr. M.C. Ortega-Liebana, Dr. M. M. Encabo-Berzosa, Dr. Jose L. Hueso*, Prof. J. Santamaria*
Department of Chemical and Environmental Engineering and Institute of Nanoscience of Aragon (INA)
Campus Rio Ebro, R+D Building, University of Zaragoza
C/Mariano Esquillor s/n, 50018, Zaragoza, Spain
E-mail: jlhueso@unizar.es; jesus.santamaria@unizar.es

[b] Dr. M.C. Ortega-Liebana, Dr. M. M. Encabo-Berzosa, Dr. Jose L. Hueso*, Prof. J. Santamaria*
Networking Research Center on Bioengineering, Biomaterials and Nanomedicine (CIBER-BBN), 28029 Madrid, Spain

[c] Dr. A. Casanova, Dr. D. Pereboom, Prof. J.O. Alda
Department of Pharmacology and Physiology
Zaragoza Medical School, University of Zaragoza
C/ Domingo Miral s/n, 50009, Zaragoza, Spain

Supporting information for this article is given via a link at the end of the document.

range with a simultaneous role as i) biomarkers that can be readily internalized by tumoral cells and ii) agents capable of in situ generation of highly reactive oxidative species (ROS) after illumination with an NIR source to induce necrosis of the irradiated cells. We also show the potential of flow imaging cytometry to detect in situ the different ROS species locally formed upon NIR stimulation of CNDs and the different type of damage and death induced.

RESULTS AND DISCUSSION

Synthesis and characterization of EDTA-derived carbon nanodots

The hydrothermal carbonization (HTC) process for the synthesis of the N-CNDs is summarized in the Figure 1a. HTC is regarded as a direct and efficient synthetic approach that works through polymerization and carbonization reactions. It has been widely applied to synthesize a wide variety of materials due to the high reactivity of the reactants, easy control of the solution parameters and limited energy consumption. The process typically proceeds via a sequential number of steps including polymerization and carbonization of organic precursors (Figure 1a). Hu el al.[43] suggested a detailed mechanism proceeding *via* four stages, including dehydration, polymerization, carbonization, and passivation. They claimed in their study that the molecules assembled as a result of hydrogen bonding. Then, during heating (dehydration), polymerization occurred, leading to a short single burst of nucleation. The resulting nuclei then intergrew by the diffusion of solutes toward the particle surfaces.

In our work, EDTA, a low-cost and naturally abundant amino-acid like compound was utilized as single-source precursor for this purpose. Upon heating, the polymer nanoparticles that begin to form from the initial stage of the EDTA dehydration process shrink due to continuous dehydration and C=C and C=N bonds are formed. In parallel, aromatic clusters are formed and when their concentration reaches a critical super-saturation point, nucleation of carbon nanodots takes place after multiple aggregation events[43]. Finally, the polymers disappear and CNDs remain[43]. TEM analysis shows the presence of crystalline N-CNDs with clear lattice fringes and average sizes of 2.9 ± 0.5 nm (Figure 1b and Figure S1).

Recently, Papaioannou et al.[44] suggested that this crystalline structure can be induced due to the role of the polymeric units as hot spots during the HT process and the temperature gradients existing in the autoclave. Likewise, these authors postulated that the partial gasification of organic precursors like EDTA under subcritical conditions (in the presence of in situ generated CO/CO_2) leads to the formation of crystalline nuclei via CO_2 reduction under autogenic pressures induces onto the surfaces of the hot spots in a sort of chemical vapor deposition (CVD) mechanism[44].

The UV-Vis-NIR absorption spectrum displayed in Figure S2 reveals the maximum at 240 and 360 nm, typically associated to π→ π* (C=C) transitions and n→ π* (conjugated C-O/C-N) transitions, respectively[45]. Figure 1c reveals that the N-CNDs exhibit an excitation-dependent emission. As the excitation wavelength increases, the emission spectra progressively red-shifts. This typical response arises from the radiative band-edge recombination (electron-hole pair recombination) upon absorption of a photon with energy superior to the bandgap energy).

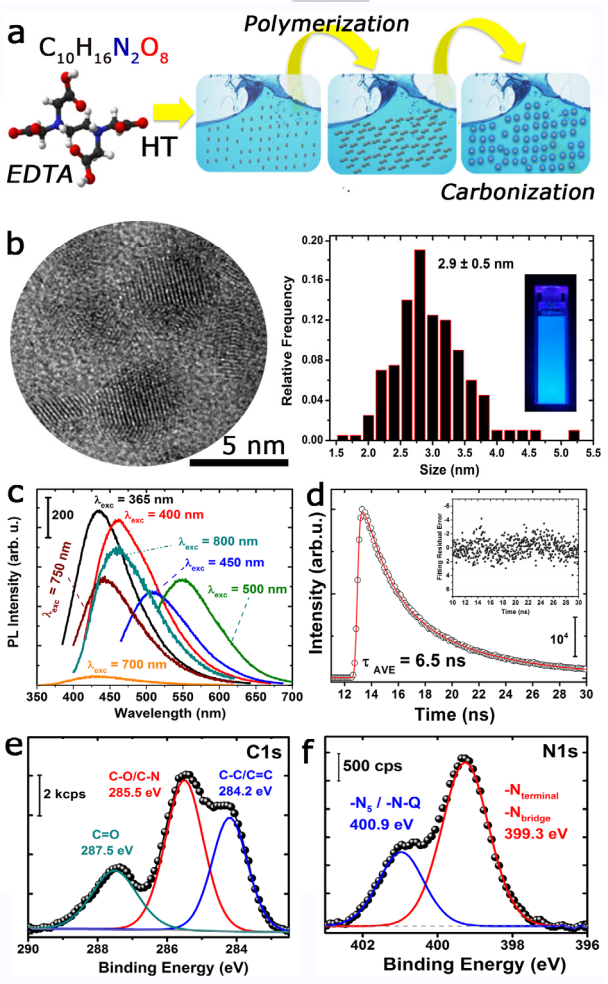

Figure 1. Synthesis and characterization of the N-CNDs: a) Scheme of the Hydrothermal Carbonization steps to convert EDTA into N-doped CNDs; b) High-Resolution TEM image of the retrieved N-CNDs and their corresponding average size distribution (inset: digital image of an aqueous suspension containing N-CNDs and excited by a UV lamp (λexc = 365 nm); c) Wavelength-dependent photoluminescence spectra of the N-CNDs; d) Time-resolved fluorescence decay curve of the N-CNDs at an excitation wavelength of 470 nm (inset: Residual error after a triple-exponential fitting); e) X-ray Photoemission spectrum and fittings corresponding to the C1s region of the N-CNDs; f) X-ray Photoemission spectrum and fittings corresponding to the N1s region of the N-CNDs..

The Quantum Yields corresponding to these samples are close to 17% (see Experimental Section) in good agreement with reports of previous CNDs synthesized under HTC conditions. Remarkably, it is worth mentioning that these N-CNDs also exhibit upconverting behaviour (i.e. the emission of photons at higher wavelengths than the excitation wavelength) in the NIR

excitation range (750-800 nm). This effect has been attributed to the presence of additional energy π-levels near the LUMO levels of carbon promoted by N doping heteroatoms that facilitate the sequential absorption of less energetic photons that can be re-excited by a second photon to higher unoccupied levels prior to the radiative recombination step[2, 38, 39, 46-48]. This enhanced intra-molecular charge transfer efficiency accompanied by an extended light absorption capability in the whole spectrum represents a very attractive optical feature to be exploited in the NIR biological window where the absorption of light by water, tissues and hemoglobine is minimized. Still, the debate regarding the exact origin of this upconversion mechanism in carbon-based nanoparticles is open and not completely unravelled since additional fluorescent compounds linked to the carbogenic cores may be participating on the observed optical response[38, 49-52].

Time-resolved photoluminescence decay measurements adjusted well to a sum of three-exponential functions wit a lifetime average of 6.5 ns. The shortest fitting components have been previously attributed to intrinsic recombination of populated core states whilst the longer (slower) fitting components have been usually related to surface defects that give rise to surface traps and surface states[38, 53, 54]. The evaluation of the surface functional groups by XPS further confirms enrichment on pyridinic and terminal amines[38, 55, 56] as shown in Figure 1f for the N1s region and by the major presence of C-O/C-N bonds in the C1s region (Figure 1e). Therefore, a carbogenic core enriched on the surface with functional groups containing N heteroatoms seems to be the most plausible configuration for the N-CNDs retrieved from EDTA by HTC[38, 56, 57].

Evaluation as bioimaging agents in the visible-NIR range

The upconversion capabilities of the N-CNDs upon excitation in the NIR range (700-1000 nm) appear especially attractive since this light in this spectral region presents less photo-damage for living organisms and most importantly has a much deeper tissue penetration than visible light. In our work, the N-CNDs were first tested as potential biomarkers in the presence of different cell lines. Confocal images displayed in Figure 2 corroborate that even though N-CNDs internalization was observed in all cellular types, the uptake from the tumoral cell lines (U251MG and HeLa) was much more relevant at shorter periods of time (4h and 24 h), especially when the lower concentrations of N-CNDs were selected (50 μg/mL). Previous studies have attributed these differences to the higher negative charge of surface of cancer cells[5]. The CNDs were preferentially located at the cytoplasm. Three-dimensional histogram images of the cells confirmed the complete internalization. The AlamarBlue® assays revealed a high biocompatibility of the N-CNDs at the different studied doses and time points, observing high U251MG viabilities even for very high concentrations of CNDs (e.g. viability around 80% compared to control (untreated cells), for doses of up to 500 μg/mL, after 48 h of culture, Figure 2).

The role of these N-CNDs as potential NIR-triggered photodynamic therapeutic agents was evaluated in U251MG cells using flow cytometry. This technique is extremely allows to monitor cytotoxic responses to photosensitization while simultaneously determining the intracellular production and accumulation of reactive oxidative species (ROS) using suitable reporting molecules[58, 59]. In particular, the intracellular generation of superoxide anion ($^{\bullet}O_2^-$) and hydrogen peroxide (H_2O_2) were detected using hydroethidine (HE) and dihydrorhodamine 123 (DHR123), respectively[58-60] (see Figures 3a-3b, Experimental Section and Figures S3-S6). In comparison with control experiments carried out in the absence of N-CNDs, the presence of both reactive species indicative of intracellular generation of ROS increased upon NIR laser irradiation and in a dose-dependent manner regarding the concentration of N-CNDs (Figure 3a-3b). It is noteworthy that the NIR laser irradiation increased the production of both ROS species even in the absence of N-CNDs. However, the oxidative stress was much more pronounced upon NIR laser irradiation, with ROS production rates that were more than doubled (for both superoxide anion and hydrogen peroxide) compared to the samples without NIR irradiation.

The detection of these ROS intermediates and others such as singlet oxygen[19] has been previously reported for other carbon-based nanosystems [14, 20-22, 61-68]. The generation of superoxide anions ($^{\bullet}O_2^-$) is assisted by the electron donor character of the N-CNDs that are able to reduce the intracellular O_2 present in the cells[21, 69] (Figure 3b and Figure S4). Given the high reactivity of this radical, it will rapidly lead to a series of cascade reactions involving the generation of non-radical ROS such as H_2O_2 (Figure 3a and Figure S4) either through the formation of peroxide intermediates[21] or with the assistance of superoxide dismutases (SOD) activated as ROS scavengers by cells[60] (Figure S4). Hence, N-CNDs can generate additional reactive hydroxyl radicals through the interaction of both species[21] ($^{\bullet}O_2^- + H_2O_2 \rightarrow O_2 + {}^{\bullet}OH + OH^-$) or by specific redox processes with H_2O or H_2O_2 (Figure S6)[70, 71]. Therefore, it is interesting to note that the N-CNDs react preferentially following a PDT type I mechanism typically observed in hypoxic conditions of tumoral cells. NIR light activation promotes an electron transfer mechanism. This performance differs from other organic photosensitizers (i.e. chlorine e6) that require an oxygen-rich ambient to generate ROS (PDT type II)[69].

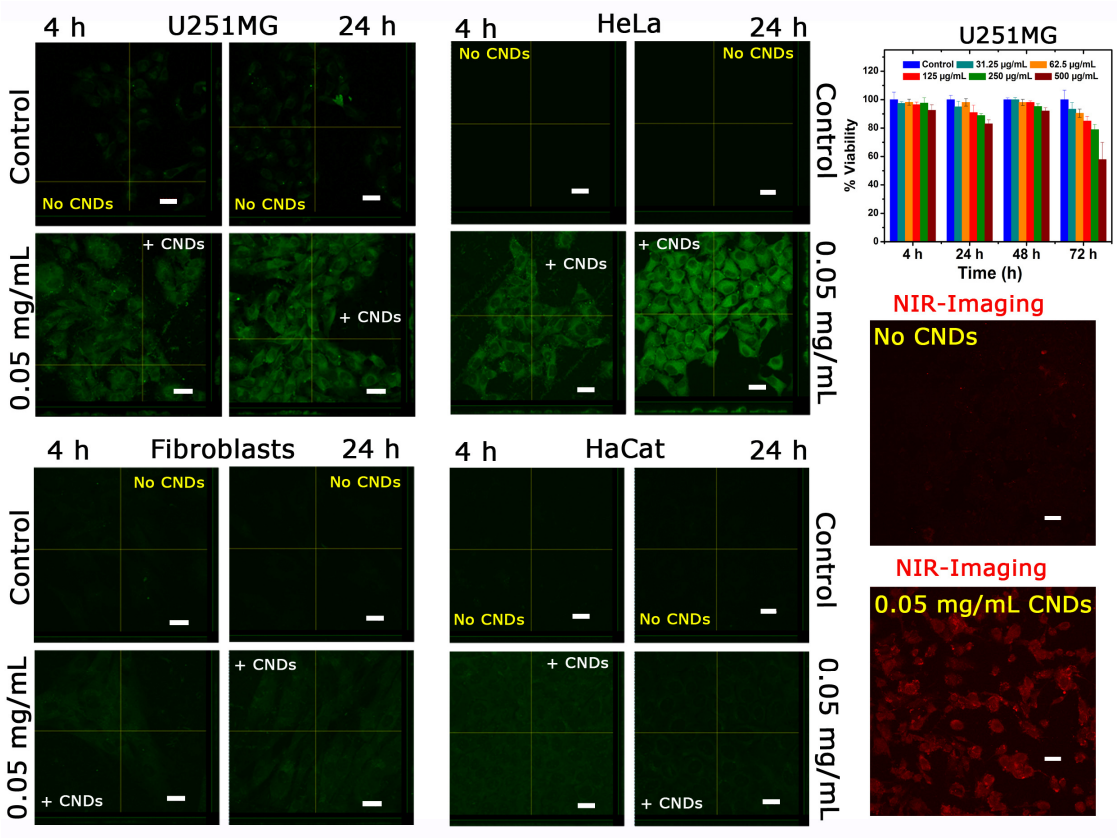

Figure 2. N-CNDs as biomarkers: Confocal images of different cells after 4 h and 24 h of incubation with 0.05 mg/mL of N-CNDs including the three dimensional histogram images; Excitation wavelengths: 473 nm; Right top panel corresponds to the evaluation of the cytotoxicity of different N-CNDs concentrations on U251MG human glioma cells after up to 72 hours of internalization and the right bottom images correspond to two-photon imaging of those cells after 24 h incubation and irradiating with a 740 nm excitation wavelength. All scale bars in the confocal images correspond to 20 microns.

Furthermore, flow cytometric analysis using Annexin V-FTIC / propidium iodide (PI) double staining was performed after 10 min NIR laser irradiation of U251MG glioma cells to determine the specific type of cell death induced by the in situ generated ROS species (Figure 3c-3e). In contrast to electron spin resonance (EPR) or electrochemical methods, this optical method exhibits several advantages for the in situ monitorization of ROS and permits high-throughput screening and imaging of cells[58, 68]. It was observed that NIR light irradiation on these tumour cells mostly caused necrosis in a short time, and that the proportion of necrotic cells was significantly higher than the others (i.e. apoptotic, etc). The major changes and damage observed in the cancer cells can be attributed to the disruption induced by ROS thereby dramatically affecting their permeability and inducing their death. The presence of N-CNDs or the NIR laser irradiation individually resulted in a slight reduction in cell viability, increasing the population of necrotic cells. More specifically, an N-CNDs dose of 100 µg/mL produced less necrotic increase than that observed following NIR laser irradiation in the absence of N-CNDs.

The combination of N-CNDs treatment (100 µg/mL) and laser irradiation had a synergistic effect, being able to induce necrosis in half of the U251MG population. At higher doses of N-CNDs (400 µg/mL), the decrease in cell viability can be mainly attributed to the increase in the population of necrotic cells, but also to an increase in early apoptosis that was not observed with the lower concentration (Figure 3f). The cell death effects seem to be dose dependent and increased strongly under 800 nm laser irradiation. Previous works with graphene-like dots claimed an additional photothermal effect as co-responsible for the photoinduced apoptotic death of tumoral cells caused by locally induced temperature increments [1, 19, 48]. Other N-CNDs required the combined effect of attached specific (chemo)-prodrugs[1, 22].Instead, the N-CNDs developed in this work act as photosensitizers capable of remote triggering by deeper penetrating NIR light, to convert light into ROS species that cause extensive cell death, (mainly through necrosis) likely caused by a variety of causes: damage to protein, DNA and lipids, and disruption of the correct functions of mitochondria[1, 19, 48]. In addition, the N-doped CNDs appear to exhibit a successful and preferential internalization in tumoral cells and also play a dual role as NIR responsive biomarkers. All of these characteristics make them highly promising materials in the emerging theranostics field.

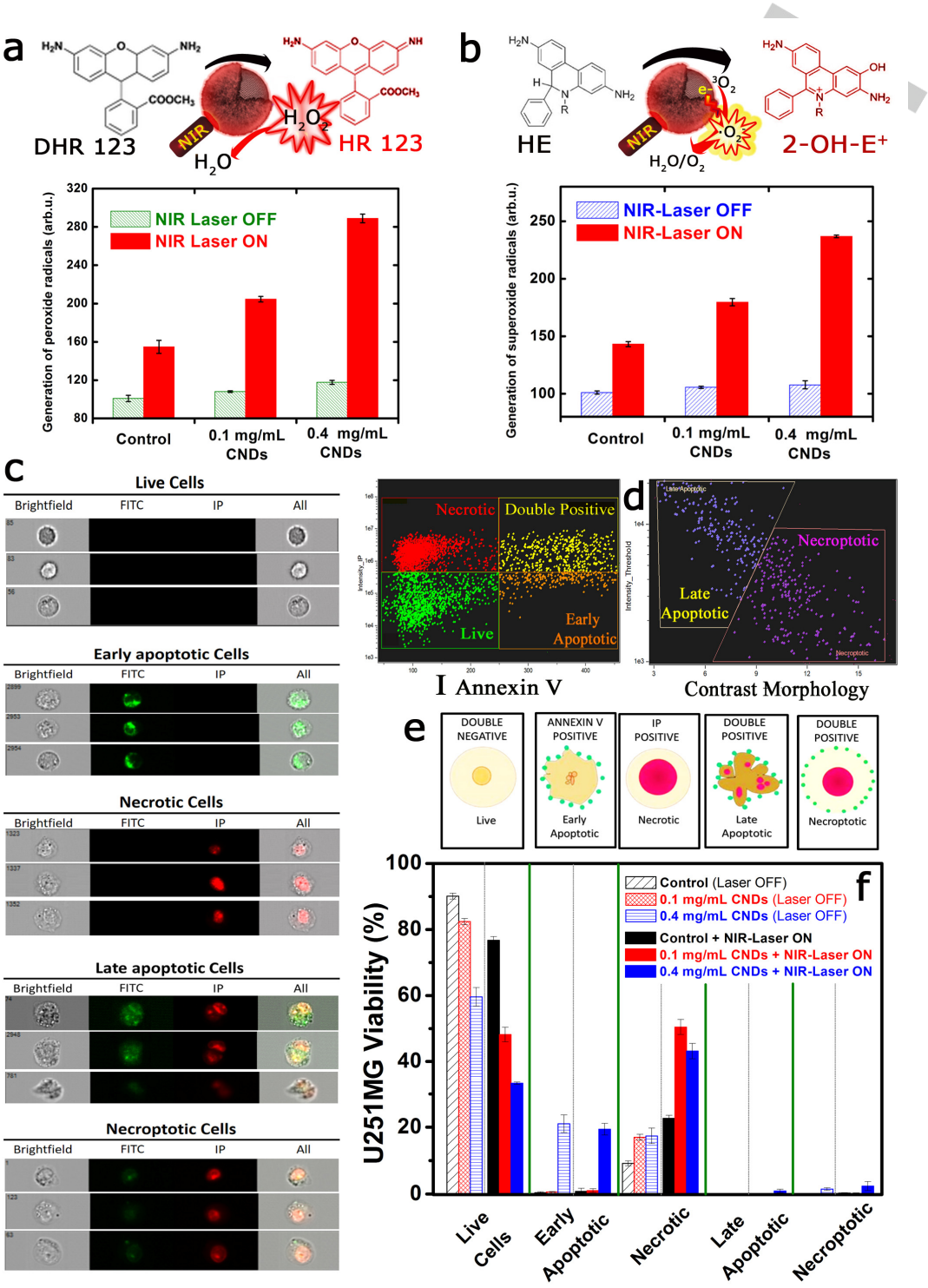

Figure 3. Analysis of N-CNDs as NIR-responsive PDT agents: a) Colorimetric essays carried out to detect the in situ generation of hydrogen peroxide before and after NIR laser irradiation of U251 MG cells incubated with different concentrations of N-CNDS, using DHR 123 as fluorescent marker; b) Colorimetric detection of superoxide radicals before and after irradiation of U251 MG cells incubated with different concentrations of N-CNDS, using HE as fluorophore; c) Snapshots of individual U251MG cells acquired by flow cytometry accounting for the main morphology changes and staining levels acquired depending on the type cell damage; d) Analysis of the different types of cell deaths identified by flow cytometry after 10 minutes of NIR irradiation of U251MG cells incubated with 0.1 mg/mL CNDs and doubly-stained with Annexin V and Propidium Iodide (PI); e) Schematic representation of the change of morphology and staining associated to each specific type of cell death identified in the flow cytometer and depicted in c); f) Cell death analysis identified by flow cytometry for U251MG cells after their incubation with different N-CNDs concentrations and after being subjected or not to NIR irradiation.

Experimental Procedures

Materials

Ethylenediaminetetraacetic acid (EDTA, 99.995%) was obtained from Sigma-Aldrich. All chemicals were of analytical purity grade and were used without further purification. 10 KDa molecular weight cut off (MWCO) membranes (Amicon Ultra-15, Millipore) were also obtained from Sigma-Aldrich.

Synthesis of Carbon Nanodots

N-doped carbon nanodots (N-CNDs) were easily synthesized in one-step by hydrothermal method. Briefly, 1M solution of EDTA, as the carbon source, and 10 mL triple distilled water were mixed in a beaker with a magnetic blender, the solution was then transferred into a 25 mL Teflon-lined stainless-steel autoclave and was heated at a constant temperature of 260 ºC for 4 hours. The resulting solution was cooled at room temperature and was centrifuged at 6000 rpm for 10 min to remove agglomerated particles. The supernatant containing carbon nanomaterials was filtered through a 0.10 mm PTFE membrane (WhatmanTH) membrane to further remove large particles. The brownish yellow supernatant was then dialyzed against ultrapure water through a dialysis membrane for 5 h. This synthesis condition corresponds to the minimum reaction times and temperatures at which CNDs were obtained. Lower T or times failed to retrieve homogeneous and reproducible luminescent nanocarbons with the desired optical response.

Cell Culture

The tumoral cell lines U251MG and HeLa cells, and the somatic cell lines (human dermal fibroblast and HaCat keratinocytes) were cultured in Dulbecco's modifies Eagle's medium (DMEM, Gibco) supplemented with 10% fetal bovine serum (FBS, Gibco), 1% penicillin/streptomycin and 1% amphotericin at 37 °C under a 5% CO_2-humidified atmosphere with normoxic conditions. Meanwhile, osteoblasts were cultured in OGM™ medium (Lonza) under the above mentioned conditions.

Cytotoxicity evaluation

The *in vitro* cytotoxicity of the N-CNDs was determined by AlamarBlue® assay. For that, U251MG cells were seeded onto 96-well microplate at a density of 5 x 10^3 cells per well and cultured for 24 h. After that, culture medium was removed and cells were treated with 100 µL of different N-CNDs solutions in DMEM (31.25 µg/mL to 1 mg/mL (serial dilutions)) and were cultured for another 4, 24, 48 and 72 h. Cells without exposure to N-CNDs were used as control. At the selected incubation times, treatments were removed and U251MG cells were washed twice with PBS, following by the addition of DMEM containing 10% (v/v) AlamarBlue®. Culture plates were maintained under normoxic conditions in a 5% CO_2 incubator at 37 °C during 3 h. Afterwards, fluorescence changes were evaluated at 530/590 nm excitation/emission wavelengths using a Synergy HT (Biotek).

Bioimaging confocal experiments

The internalization and *in vitro* emission of N-CNDs was evaluated in different cell types at two different incubation times (4 and 24 h) and two concentrations (50 and 400 µg/mL). The N-CNDs solutions used in the assays were obtained by diluting the stocks in culture cell medium. The final concentration of water in the final medium employed did not cause any osmotic imbalance. First, different cells types were cultured as mentioned above. Briefly, cells were seeded on sterile cover-slips at a density of 40000 cells per well and were incubated during 24 h to facilitate substrate adhesion. After that, medium was removed and N-CNDs suspensions were added to cultured cells. At the incubation times selected (4 and 24 h), the medium containing N-CNDs was removed and cells were washed twice with PBS, in order to eliminate non-internalized nanoparticles, and fixed with 4% paraformaldehyde. Subsequently, the cover-slips were mounted and the samples were observed in an Olympus FV10-i Oil Type confocal microscopy with a laser excitation source at 473 nm and analyzed with the microscopy software. Analogous settings were employed for both the control experiments (without N-CNDs) and the treated samples.

Oxidative stress determination

The intracellular general ROS production was detected by the oxidation-sensitive fluorescent probe dye. Specifically, hydrogen peroxide production was measured using Dihydrorhodamine 123 (DHR, Sigma Aldrich) and superoxide anion formation was studied using Hydroethidine (HE, Sigma Aldrich). It is important to remark that ROS production measurement was carried out in live cells, which were stained with propidium iodide (0.025 mM, Sigma Aldrich) incubation during 15 min. After that, individual fluorescence cell intensity was analyzed using an ImageStreamX image cytometer (Amnis, Seattle, WA), measuring the emission between 520-617 nm under an excitation wavelength of 488 nm. Briefly, U251MG were seeded onto 48-well microplates and incubated with N-CNDs at two different concentrations (100 and 400 µg/mL) during 24 h. After that, cells were irradiated during 10 min using a NIR laser (808 nm, 2 W/cm^2). Subsequently, cells were stained with DHR123 or HE, and cellular fluorescence intensity was analyzed with an ImageStreamX image cytometer, measuring the fluorescence emission at 480-560 nm (DHR) or 595-660 nm (HE) under 488 nm excitation. Cells without nanoparticles and non-irradiated were used as control. The effect of N-CNDs without laser irradiation and laser without N-CNDs incubation was also evaluated.

Cell death analysis

The cell death study was based on cells morphological analysis using double labeling with annexin V and propidium iodide (AV/IP), that allows to divide cells into four populations: live cells (negative for both dyes), necrotic (AV-, IP+), early apoptotic (AV+, IP-) and late apoptotic/necroptotic cells (positive for both dyes). In summary, cells were incubated with the N-CNDs at the concentrations of 100 and 400 µg/mL and subsequently irradiated with a NIR laser (808 nm, 2 W/cm^2) coupled to fiber collimator (THORLABS F220SMA-

780, 780 nm, f=11.07mm) during 10 min. Cells without nanoparticles and not irradiated were used as control. Also the effects of N-CNDs without laser and laser effect without N-CNDs incubation were studied. Cytometer results were analyzed using the *IDEAS*® software that allows the differentiation between late apoptotic and necroptotic populations through "Contrast_Morphology Vs Intensity_Threshold" morpho-cytometric parameters separation.

Statistical analysis

All the experiments were repeated at least six times as independent experiments. The results are represented as mean +/− standard deviation. The normal distribution was tested by the Kolmogorov-Smirnov test; Statistical significance was set at $p<0.05$. For the parametric data a multiple comparison was made with ANOVA followed by a comparison of two by two with the t-test. For no parametric data Kruskal Wallis were performed followed of the U Mann Whitney comparison test.

Characterization techniques

The morphologies and particle size distributions were determined by transmission electron microscopy (TEM) (FEI Tecnai T20 and F30, operated at 200-300 kV, respectively). To prepare the samples, the nanoparticle suspensions were diluted with water prior to casting on a holey carbon TEM grid. The functionalization of the CNDs surface was analyzed by X-ray photoelectron spectroscopy (XPS) with an Axis Ultra DLD (Kratos Tech.). A monochromatic Al Kα source (1486.6 eV) was employed with multiple runs at 12 kV, 10 mA and pass energy of 20 eV was used. The binding energies were calibrated to the internal C1s (284.3 eV) standard. Analyses of the peaks were performed with CasaXPS software, using a weighted sum of Lorentzian and Gaussian component curves after Shirley background subtraction. Steady-state fluorescence emission spectra were collected on a JASCO FP-6500 spectrofluorometer equipped with a 450 W xenon lamp for excitation, with temperature controller ETC-273T at 25 °C, using 5×10 mm cuvettes and a LS55 Fluorescence Spectrometer (PerkinElmer) equipped with a xenon arc lamp as the light source and a quartz cell (10 x 10 mm). The excitation wavelengths used in the experiments to record the emission spectra were 400 and 740 nm. Both excitation and emission slits were 3 nm.

The fluorescence quantum yields Φ of the different CNDs in aqueous solution were computed according to the equation: $\Phi_S = \Phi_R \times F_S \times (1\text{-}10^{-AR\ (\lambda ex)}) \times n_S^2 / F_R \times (1\text{-}10^{-AS\ (\lambda ex)}) \times n_R^2$). The subscript S refers to the CND samples, R stands for the selected reference fluorophore (quinine sulfate, 0.1 M H_2SO_4) with known quantum yield (0.54), F stands for the corrected, integrated fluorescence spectra, $A(\lambda_{exc})$ denotes the absorbance at the used excitation wavelength λ_{exc}, and n represents the refractive index of the solvent. To minimize inner filter effects, the absorbance at the excitation wavelength λ_{exc} was kept under 0.1. The measurements were performed using 10 mm optical path length cuvettes under right-angle (L-) arrangement and 'magic angle' conditions. The averages and standard uncertainties of Φ are computed from independent Φ measurements (2 conc. of sample × 2 conc. of reference × 2 excitation wavelengths λ_{exc}).Fluorescence decay traces of the different CNDs were recorded in the Time Correlated Single Photon Counting (TCSPC) mode using the FluoTime 200 fluorometer (PicoQuant, GmbH). Briefly, the samples were excited by a 405 nm Picosecond Pulsed Diode Laser (Edinburgh EPL405) with a 10 MHz repetition rate. The full width at half maximum of the laser pulse was ~ 90 ps. The fluorescence was collected after crossing through a polarizer set at the magic angle, and a 2 nm bandwidth monochromator. Fluorescence decay histograms were collected using a TimeHarp200 board, with a time increment per channel of 36 ps, at the emission wavelengths of 450, 460, and 470 nm. The histograms of the instrument response function (IRF) was determined using LUDOX scatterer, and sample decays were recorded until they typically reached 2×10^4 counts in the peak channel, since it is well known that complex decays can be well described by the simplest exponential models if the fitting is carried out from experimental data with a low number of CPC.

CONCLUSIONS

In summary, we have synthesized nitrogen-doped carbon dots as photo-enabled therasnostic agents. These CNDs synthesized by hydrothermal carbonization of a single molecular precursor (EDTA) exhibit an outstanding upconverting response in the Near-Infrared Range that has enabled their simultaneous application as NIR biomarkers with preferential internalization in tumoral cells and their remote NIR activation to efficient generate ROS species to induce cell death. Finally, in this work Flow Cytometry has been thoroughly exploited not only to in situ identify the ROS species but also to quantify cell death types on a cell to cell basis after illumination with a NIR source.

Acknowledgements

The authors acknowledge the European Research Council for funding through an advanced grant research project (HECTOR grant number 267626; CADENCE grant number 742684) and a CIG-Marie Curie Reintegration Grant (NANOLIGHT REA grant number 294094). The TEM measurements were conducted at the Laboratorio de Microscopias Avanzadas, Instituto de Nanociencia de Aragon, Universidad de Zaragoza, Spain. The synthesis of materials has been performed by the Platform of Production of Biomaterials and Nanoparticles of the NANOBIOSIS ICTS, more specifically by the Nanoparticle Synthesis Unit of the CIBER in BioEngineering, Biomaterials & Nanomedicine (CIBER-BBN). M.C.O. acknowledges the Spanish Government for an FPU predoctoral fellowship. We finally thank Dr. Ruedas-Rama for the help in the acquisition of the time-resolved decay measurements and Dr. Irusta for the XPS measurements.

Keywords: near-infrared • carbon nanodots • phototheranostics • biomarkers • reactive oxidative species

[1] K. R. Deng, C. X. Li, S. S. Huang, B. G. Xing, D. Y. Jin, Q. G. Zeng, Z. Y. Hou, J. Lin, *Small* **2017**, *13*.
[2] J. Croissant, A. Chaix, O. Mongin, M. Wang, S. Clement, L. Raehm, J. O. Durand, V. Hugues, M. Blanchard-Desce, M. Maynadier, A. Gallud, M. Gary-Bobo, M. Garcia, J. Lu, F. Tamanoi, D. P. Ferris, D. Tarn, J. I. Zink, *Small* **2014**, *10*, 1752-1755.
[3] D. Yang, G. X. Yang, P. P. Yang, R. C. Lv, S. L. Gai, C. X. Li, F. He, J. Lin, *Adv. Funct. Mater.* **2017**, *27*.
[4] H. Y. Huang, J. F. Lovell, *Adv. Funct. Mater.* **2017**, *27*.
[5] D. Wang, H. F. Su, R. T. K. Kwok, X. L. Hu, H. Zou, Q. X. Luo, M. M. S. Lee, W. H. Xu, J. W. Y. Lam, B. Tang, *Chem. Sci.* **2018**, *9*, 3685-3693.
[6] I. O. de Solorzano, M. Prieto, G. Mendoza, T. Alejo, S. Irusta, V. Sebastian, M. Arruebo, *ACS Appl. Mater. Interfaces* **2016**, *8*, 21545-21554.
[7] M. Gary-Bobo, Y. Mir, C. Rouxel, D. Brevet, I. Basile, M. Maynadier, O. Vaillant, O. Mongin, M. Blanchard-Desce, A. Morere, M. Garcia, J. O. Durand, L. Raehm, *Angew. Chem.-Int. Edit.* **2011**, *50*, 11425-11429.
[8] Z. J. Gu, L. Yan, G. Tian, S. J. Li, Z. F. Chai, Y. L. Zhao, *Adv. Mater.* **2013**, *25*, 3758-3779.
[9] L. L. Feng, S. L. Gai, F. He, Y. L. Dai, C. N. Zhong, P. P. Yang, J. Lin, *Biomaterials* **2017**, *147*, 39-52.
[10] L. L. Feng, F. He, B. Liu, G. X. Yang, S. L. Gai, P. P. Yang, C. X. Li, Y. L. Dai, R. C. Lv, J. Lin, *Chem. Mat.* **2016**, *28*, 7935-7946.
[11] T. Gao, X. Wang, L. Y. Yang, H. He, X. X. Ba, J. Zhao, F. L. Jiang, Y. Liu, *ACS Appl. Mater. Interfaces* **2017**, *9*, 24846-24856.
[12] Z. Q. Xu, J. Y. Lan, J. C. Jin, P. Dong, F. L. Jiang, Y. Liu, *ACS Appl. Mater. Interfaces* **2015**, *7*, 28346-28352.
[13] Z. Q. Xu, L. Y. Yang, X. Y. Fan, J. C. Jin, J. Mei, W. Peng, F. L. Jiang, Q. Xiao, Y. Liu, *Carbon* **2014**, *66*, 351-360.
[14] M. Nurunnabi, Z. Khatun, G. R. Reeck, D. Y. Lee, Y. K. Lee, *ACS Appl. Mater. Interfaces* **2014**, *6*, 12413-12421.
[15] M. Kim, J. Jang, C. Cha, *Drug Discov. Today* **2017**, *22*, 1430-1437.
[16] H. Huang, C. G. Li, S. J. Zhu, H. L. Wang, C. L. Chen, Z. R. Wang, T. Y. Bai, Z. Shi, S. H. Feng, *Langmuir* **2014**, *30*, 13542-13548.
[17] K. Albert, H. Y. Hsu, *Molecules* **2016**, *21*.
[18] Z. Khatun, M. Nurunnabi, M. Nafiujjaman, G. R. Reeck, H. A. Khan, K. J. Cho, Y. K. Lee, *Nanoscale* **2015**, *7*, 10680-10689.
[19] J. C. Ge, M. H. Lan, B. J. Zhou, W. M. Liu, L. Guo, H. Wang, Q. Y. Jia, G. L. Niu, X. Huang, H. Y. Zhou, X. M. Meng, P. F. Wang, C. S. Lee, W. J. Zhang, X. D. Han, *Nat. Commun.* **2014**, *5*.
[20] M. Zhang, W. T. Wang, N. L. Zhou, P. Yuan, Y. T. Su, M. N. Shao, C. Chi, F. Y. Pan, *Carbon* **2017**, *118*, 752-764.
[21] X. N. Dou, Z. Lin, H. Chen, Y. Z. Zheng, C. Lu, J. M. Lin, *Chem. Commun.* **2013**, *49*, 5871-5873.
[22] Y. L. Pang, Z. H. Mai, B. Wang, L. Wang, L. P. Wu, X. P. Wang, T. S. Chen, *Oncotarget* **2017**, *8*, 93800-93812.
[23] Y. Choi, S. Kim, M. H. Choi, S. R. Ryoo, J. Park, D. H. Min, B. S. Kim, *Adv. Funct. Mater.* **2014**, *24*, 5781-5789.
[24] P. Huang, J. Lin, X. S. Wang, Z. Wang, C. L. Zhang, M. He, K. Wang, F. Chen, Z. M. Li, G. X. Shen, D. X. Cui, X. Y. Chen, *Adv. Mater.* **2012**, *24*, 5104-5110.
[25] S. Y. Lim, W. Shen, Z. Q. Gao, *Chem. Soc. Rev.* **2015**, *44*, 362-381.
[26] K. Yang, L. Z. Feng, X. Z. Shi, Z. Liu, *Chem. Soc. Rev.* **2013**, *42*, 530-547.
[27] J. C. Ge, Q. Y. Jia, W. M. Liu, M. H. Lan, B. J. Zhou, L. Guo, H. Y. Zhou, H. Y. Zhang, Y. Wang, Y. Gu, X. M. Meng, P. F. Wang, *Adv. Healthc. Mater.* **2016**, *5*, 665-675.
[28] B. J. Geng, D. W. Yang, D. Y. Pan, L. Wang, F. F. Zheng, W. W. Shen, C. Zhang, X. K. Li, *Carbon* **2018**, *134*, 153-162.
[29] P. W. Gong, L. Sun, F. Wang, X. C. Liu, Z. Q. Yan, M. Z. Wang, L. Zhang, Z. Z. Tian, Z. Liu, J. M. You, *Chem. Eng. J.* **2019**, *356*, 994-1002.
[30] X. Bao, Y. Yuan, J. Q. Chen, B. H. Zhang, D. Li, D. Zhou, P. T. Jing, G. Y. Xu, Y. L. Wang, K. Hola, D. Z. Shen, C. F. Wu, L. Song, C. B. Liu, R. Zboril, S. N. Qu, *Light-Sci. Appl.* **2018**, *7*.
[31] M. H. Lan, S. J. Zhao, Z. Y. Zhang, L. Yan, L. Guo, G. L. Niu, J. F. Zhang, J. F. Zhao, H. Y. Zhang, P. F. Wang, G. Y. Zhu, C. S. Lee, W. J. Zhang, *Nano Res.* **2017**, *10*, 3113-3123.
[32] Q. Y. Jia, J. C. Ge, W. M. Liu, S. Liu, G. L. Niu, L. Guo, H. Y. Zhang, P. F. Wang, *Nanoscale* **2016**, *8*, 13067-13077.
[33] L. J. Luo, C. Liu, T. He, L. Y. Zeng, J. Xing, Y. Z. Xia, Y. W. Pan, C. Y. Gong, A. G. Wu, *Nanoscale* **2018**, *10*, 22035-22043.
[34] D. Y. Pan, J. C. Zhang, Z. Li, C. Wu, X. M. Yan, M. H. Wu, *Chem. Commun.* **2010**, *46*, 3681-3683.
[35] D. Y. Pan, J. C. Zhang, Z. Li, Z. W. Zhang, L. Guo, M. H. Wu, *J. Mater. Chem.* **2011**, *21*, 3565-3567.
[36] Y. H. Deng, X. Chen, F. Wang, X. A. Zhang, D. X. Zhao, D. Z. Shen, *Nanoscale* **2014**, *6*, 10388-10393.
[37] Y. J. Zhang, R. R. Yuan, M. L. He, G. C. Hu, J. T. Jiang, T. Xu, L. Zhou, W. Chen, W. D. Xiang, X. J. Liang, *Nanoscale* **2017**, *9*, 17849-17858.
[38] M. C. Ortega-Liebana, M. M. Encabo-Berzosa, M. J. Ruedas-Rama, J. L. Hueso, *Chem.-Eur. J.* **2017**, *23*, 3067-3073.
[39] B. Kong, A. W. Zhu, C. Q. Ding, X. M. Zhao, B. Li, Y. Tian, *Adv. Mater.* **2012**, *24*, 5844-5848.
[40] H. Tetsuka, R. Asahi, A. Nagoya, K. Okamoto, I. Tajima, R. Ohta, A. Okamoto, *Adv. Mater.* **2012**, *24*, 5333-5338.
[41] Y. Q. Dong, H. C. Pang, H. B. Yang, C. X. Guo, J. W. Shao, Y. W. Chi, C. M. Li, T. Yu, *Angew. Chem.-Int. Edit.* **2013**, *52*, 7800-7804.
[42] S. L. Hu, A. Trinchi, P. Atkin, I. Cole, *Angew. Chem.-Int. Edit.* **2015**, *54*, 2970-2974.
[43] Y. P. Hu, J. Yang, J. W. Tian, J. S. Yu, *J. Mat. Chem. B* **2015**, *3*, 5608-5614.
[44] N. Papaioannou, A. Marinovic, N. Yoshizawa, A. E. Goode, M. Fay, A. Khlobystoyv, M. M. Titirici, A. Sapelkin, *Sci Rep* **2018**, *8*.
[45] D. Qu, M. Zheng, J. Li, Z. G. Xie, Z. C. Sun, *Light-Sci. Appl.* **2015**, *4*.
[46] A. Gulzar, J. T. Xu, P. P. Yang, F. He, L. G. Xu, *Nanoscale* **2017**, *9*, 12248-12282.
[47] Y. Huang, F. Qiu, L. Y. Shen, D. Chen, Y. Su, C. Yang, B. Li, D. Y. Yan, X. Y. Zhu, *ACS Nano* **2016**, *10*, 10489-10499.
[48] S. Y. Lu, L. Z. Sui, J. J. Liu, S. J. Zhu, A. M. Chen, M. X. Jin, B. Yang, *Adv. Mater.* **2017**, *29*.
[49] J. B. Essner, J. A. Kist, L. Polo-Parada, G. A. Baker, *Chem. Mat.* **2018**, *30*, 1878-1887.
[50] J. Schneider, C. J. Reckmeier, Y. Xiong, M. von Seckendorff, A. S. Susha, P. Kasak, A. L. Rogach, *J. Phys. Chem. C* **2017**, *121*, 2014-2022.
[51] S. J. Zhu, X. H. Zhao, Y. B. Song, S. Y. Lu, B. Yang, *Nano Today* **2016**, *11*, 128-132.
[52] L. Shi, J. H. Yang, H. B. Zeng, Y. M. Chen, S. C. Yang, C. Wu, H. Zeng, O. Yoshihito, Q. Q. Zhang, *Nanoscale* **2016**, *8*, 14374-14378.
[53] A. Orte, J. M. Alvarez-Pez, M. J. Ruedas-Rama, *ACS Nano* **2013**, *7*, 6387-6395.
[54] M. J. Ruedas-Rama, J. D. Walters, A. Orte, E. A. H. Hall, *Anal. Chim. Acta* **2012**, *751*, 1-23.
[55] M. C. Ortega-Liebana, J. L. Hueso, S. Ferdousi, R. Arenal, S. Irusta, K. L. Yeung, J. Santamaria, *Appl. Catal. B-Environ.* **2017**, *218*, 68-79.
[56] J. L. Hueso, J. P. Espinos, A. Caballero, J. Cotrino, A. R. Gonzalez-Elipe, *Carbon* **2007**, *45*, 89-96.
[57] M. C. Ortega-Liebana, N. X. Chung, R. Limpens, L. Gomez, J. L. Hueso, J. Santamaria, T. Gregorkiewicz, *Carbon* **2017**, *117*, 437-446.
[58] M. J. Naya, D. Pereboom, J. Ortego, J. O. Alda, A. Lanas, *Gut* **1997**, *40*, 175-181.

[59] Y. Gilaberte, D. Pereboom, F. J. Carapeto, J. O. Alda, *Photodermatol. Photoimmunol. Photomed.* **1997**, *13*, 43-49.
[60] H. T. Zhao, S. Kalivendi, H. Zhang, J. Joseph, K. Nithipatikom, J. Vasquez-Vivar, B. Kalyanaraman, *Free Radic. Biol. Med.* **2003**, *34*, 1359-1368.
[61] Z. M. Markovic, B. Z. Ristic, K. M. Arsikin, D. G. Klisic, L. M. Harhaji-Trajkovic, B. M. Todorovic-Markovic, D. P. Kepic, T. K. Kravic-Stevovic, S. P. Jovanovic, M. M. Milenkovic, D. D. Milivojevic, V. Z. Bumbasirevic, M. D. Dramicanin, V. S. Trajkovic, *Biomaterials* **2012**, *33*, 7084-7092.
[62] D. Q. Chen, C. A. Dougherty, K. C. Zhu, H. Hong, *J. Control. Release* **2015**, *210*, 230-245.
[63] T. K. Ryu, S. W. Baek, R. H. Kang, K. Y. Jeong, D. R. Jun, S. W. Choi, *J. Control. Release* **2018**, *270*, 237-245.
[64] H. T. Li, Z. H. Kang, Y. Liu, S. T. Lee, *J. Mater. Chem.* **2012**, *22*, 24230-24253.
[65] X. D. Xu, P. E. Saw, W. Tao, Y. J. Li, X. Y. Ji, S. Bhasin, Y. L. Liu, D. Ayyash, J. Rasmussen, M. Huo, J. J. Shi, O. C. Farokhzad, *Adv. Mater.* **2017**, *29*.
[66] P. C. Hsu, P. C. Chen, C. M. Ou, H. Y. Chang, H. T. Chang, *J. Mat. Chem. B* **2013**, *1*, 1774-1781.
[67] C. L. Li, C. M. Ou, C. C. Huang, W. C. Wu, Y. P. Chen, T. E. Lin, L. C. Ho, C. W. Wang, C. C. Shih, H. C. Zhou, Y. C. Lee, W. F. Tzeng, T. J. Chiou, S. T. Chu, J. Cang, H. T. Chang, *J. Mat. Chem. B* **2014**, *2*, 4564-4571.
[68] F. Si, Y. Liu, K. L. Yan, W. W. Zhong, *Chem. Commun.* **2015**, *51*, 7931-7934.
[69] Z. J. Zhou, J. B. Song, L. M. Nie, X. Y. Chen, *Chem. Soc. Rev.* **2016**, *45*, 6597-6626.
[70] M. C. Ortega-Liebana, J. L. Hueso, S. Ferdousi, K. L. Yeung, J. Santamaria, *Diam. Relat. Mat.* **2016**, *65*, 176-182.
[71] M. C. Ortega-Liebana, J. L. Hueso, A. Larrea, V. Sebastiana, J. Santamaria, *Chem. Commun.* **2015**, *51*, 16625-16628.

10.1002/chem.201806307

WILEY-VCH

Entry for the Table of Contents

COMMUNICATION

Multi-tasking Dots: Carbon Nanodots retrieved from EDTA are presented as multifunctional theranostic agents with enhanced response in the NIR biological window. These N-Doped dots exhibit reduced cytoxicity and a preferential uptake by tumoral cells. Irradiation with a NIR source enables the effective imaging of cells and the simultaneous generation of ROS able to promote rapid necrosis on cancer cells. Flow cytometry enables a rapid and accurate cell per cell death analysis.

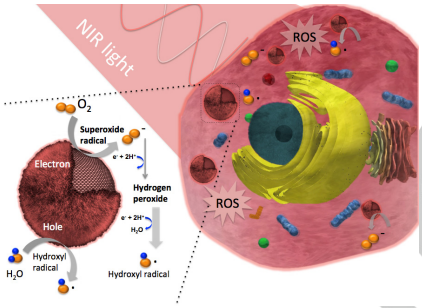

M.C. Ortega-Liebana, M. M. Encabo-Berzosa, A. Casanova, D. Pereboom, J.O. Alda, Jose L. Hueso, J. Santamaria**

Page No. – Page No.

Upconverting Carbon Nanodots from EDTA as Near-Infrared Activated Phototheranostic Agents